

Structure and stability of borohydride on Au(111) and Au₃M(111) (M = Cr, Mn, Fe, Co, Ni) surfaces

メタデータ	言語: English 出版者: 公開日: 2015-03-18 キーワード (Ja): キーワード (En): 作成者: Arevalo, Ryan Lacdao, Escano, Mary Clare Sison, Wang, Andrew, Kasai, Hideaki メールアドレス: 所属:
URL	http://hdl.handle.net/10098/8734

Structure and stability of borohydride on Au(111) and Au₃M(111) (M = Cr, Mn, Fe, Co, Ni) surfaces

Cite this: *Dalton Trans.*, 2013, **42**, 770

Ryan Lacdao Arevalo,^{a,b} Mary Clare Sison Escaño,^a Andrew Yu-Sheng Wang^c and Hideaki Kasai^{*a}

We study the adsorption of borohydride on Au and Au-based alloys (Au₃M with M = Cr, Mn, Fe, Co, and Ni) using first-principles calculations based on spin-polarized density functional theory. Favorable molecular adsorption and greater adsorption stability compared to pure Au are achieved on Au₃M alloys. For these alloys, there is an emergence of unoccupied states in the surface d band around the Fermi level with respect to the fully occupied d band of pure Au. Thus, the derived antibonding state of the sp–d interaction is upshifted and becomes unoccupied compared to pure Au. The B–H bond elongation of the adsorbed borohydride on these alloy surfaces points to the role of surface-parallel (d_{xy} and $d_{x^2-y^2}$ states) components of the d-band of the alloying metal M, most pronouncedly in the cases of M = Co or Ni. On the alloy surfaces, B binds directly with the alloying metal, unlike in the case of pure Au where the surface bonding is through the H atoms. These results pose relevant insights into the design of Au-based anode catalysts for the direct borohydride fuel cell.

Received 23rd September 2012,
Accepted 5th November 2012

DOI: 10.1039/c2dt32226a

www.rsc.org/dalton

1. Introduction

Hydrogen has been foreseen as a viable source of energy through hydrogen fuel cells.^{1–4} However, difficulties arise, especially for small-scale power applications, due to issues on hydrogen storage and gas handling safety concerns.⁵ Improvements were obtained through the “direct feeding” of liquid hydrogen-rich fuels such as borohydride to the anode. This direct borohydride fuel cell (DBFC) is a very promising power source for the future because of its high power densities for portable power applications.^{6–29} However, its efficiency and power density are limited in part by the lack of an effective catalyst for borohydride oxidation.^{7–9}

Numerous experimental studies have been carried out on the oxidation of borohydride on pure (Pt, Pd, Au, Ag, Rh, Ir) and alloy (Pt–M, M = Au, Ag, Ru, Ni, Ir, Bi) catalysts using voltammetric, amperometric, rotating electrode, and *in situ* mass and FTIR methods.^{20–29} Among the possible candidates for use as DBFC anodes, Au is uniquely capable of producing almost 100% coulombic efficiency.^{18,19} However, high overpotential is necessary to achieve an appreciable rate of

borohydride oxidation on the Au surface.^{18,19} Interestingly, recent experiments have shown that alloying Au with 3d transition metals can effectively reduce the overpotential for the oxidation of the borohydride anion and such Au–3d alloys have higher catalytic activity than Au.^{30–32} However, the electronic effect of 3d transition metals as alloying components for these alloy systems on the oxidation of borohydride is not understood. Such fundamental understanding of the interaction of borohydride with surfaces is important to efficiently utilize the high hydrogen density of the borohydride molecule.

First principles calculations based on density functional theory (DFT) were previously shown to corroborate the experimental findings on borohydride oxidation. For the case of Pt(111), borohydride was found to dissociate to BH_{ads} and 3H_{ads} fragments (ads denotes surface-bound species).^{33,34} Surface diffusion of H_{ads} and associative desorption to H₂ are very likely which explains the experimental observation of high H₂ evolution on Pt. For the case of Au, the low adsorption energy of borohydride corresponds to the experimental finding that the oxidation of borohydride requires high overpotential.^{33,35} Thus, DFT studies on the structure and energetics of borohydride on different catalysts can be used for screening desirable catalysts for borohydride oxidation.

In this paper, we provide for the first time, theoretical insights into the electronic effect of alloying Au with 3d transition metals on the adsorption of borohydride and show the importance of an unoccupied 3d orbital on the stability of borohydride on the surface and the orbital-specific effect on borohydride adsorption structure. These results are

^aDepartment of Precision Science & Technology and Applied Physics, Osaka University, 2-1 Yamadaoka, Suita, Osaka 565-0871, Japan.

E-mail: kasai@dyn.ap.eng.osaka-u.ac.jp

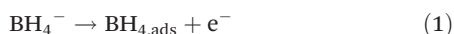
^bOn leave from: Department of Physical Sciences, Philippine Normal University, Manila 1000, Philippines

^cDepartment of Chemical and Biological Engineering, The University of British Columbia, Vancouver, BC V6T 1Z3, Canada

indispensable in the design of Au-based anode catalysts for the direct borohydride fuel cell.

2. Computational model

The adsorption of the borohydride anion (BH_4^-) has been experimentally discussed on both noble and non-noble metal catalysts^{18,20,25–29,36,37} and was found to be accompanied by the simultaneous transfer of an electron to the electrode, as shown by eqn (1).



The adsorption of borohydride on metal surfaces can be modeled in an overall neutral unit cell. This model has also been utilized in other related DFT studies for borohydride^{33–35,38,39} and for oxidative adsorption of other anions like BF_4^- and OH^- .^{40–42}

The stable configuration of the adsorbed borohydride ($\text{BH}_{4,\text{ads}}$) was determined by exhausting the possible orientations on the surface of a four-layer slab. This includes the H-up and H-down orientations (Fig. 1) of the tetrahedral borohydride with B at the high symmetry sites on the surface (top, bridge, hcp hollow and fcc hollow sites), and in-plane rotation. The adsorbate and the top two layers of the slab were fully relaxed in all directions while the bottom two layers were held fixed at their bulk structure. Each slab is separated by ~ 15.0 Å of vacuum, which is large enough to avoid the surface atom interaction along the z axis with neighboring unit cells. The electric dipole correction layer in the vacuum area was used to cut the dipole interactions between the repeated image layer systems. The adsorption energy on each metal was computed by taking the difference between the total energy of the borohydride-slab system in the lowest energy adsorption site and the summed energy of the relaxed clean surface and the gas-phase borohydride.

Spin polarized density functional theory calculations were implemented *via* the Vienna *ab initio* simulation package

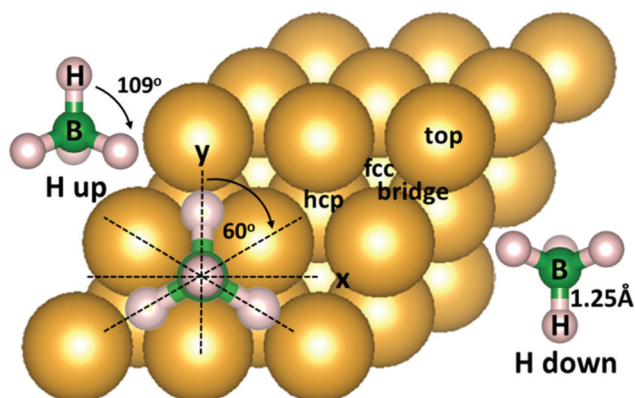


Fig. 1 The stable configuration of adsorbed borohydride ($\text{BH}_{4,\text{ads}}$) was determined by initially placing the tetrahedral borohydride in H-up and H-down orientations with B at the high symmetry sites on the surface (top, bridge, hcp hollow and fcc hollow sites) and rotating the molecule on the xy plane.

(VASP).^{43–46} The interaction between ions and electrons was described using the projector augmented wave (PAW) method.^{47,48} Plane wave basis sets were employed with an energy cut-off of 400 eV. The exchange–correlation term was described using generalized gradient approximation (GGA) based on the Perdew–Burke–Ernzerhof (PBE) functional.^{49,50} The surface Brillouin zone integrations were performed on a grid of $(4 \times 4 \times 1)$ Monkhorst–Pack k -points⁵¹ using a Methfessel–Paxton smearing⁵² of $\sigma = 0.2$ eV. A conjugate-gradient algorithm⁵³ was used to relax the ions into their ground state. The convergence of numerical results with respect to the slab thickness, the kinetic energy cut-off and the k -point was established.

3. Results and discussion

3.1 Borohydride on Au(111)

We present the interaction of borohydride on a pure Au(111) surface to make relevant comparisons with Au alloys. The calculated lattice constant for fcc Au is 4.18 Å, in excellent agreement with another DFT study.³³ The stable adsorption configuration of borohydride on Au(111) is shown in the inset of Fig. 2. Borohydride adsorbs on the surface with B at the hollow site and H atoms at the top sites in the H-up orientation. The B–H bond length is 1.26 Å, which is in very close agreement with other DFT studies.^{33,35} This lies within the B–H bond length (1.26–1.49 Å) previously reported for the case of molecularly adsorbed borohydride.^{33,39} The calculated adsorption energies for $\sim 1/9$ and $\sim 1/16$ monolayer adsorbate coverages are -1.69 eV and -1.83 eV respectively. This shows the enhanced repulsive interaction between the adsorbates as the coverage is increased. The adsorption of borohydride on Au is the weakest among all the transition metals previously studied.^{33–35,38,39} This shows the property of Au being the most noble of all metals.⁵⁴

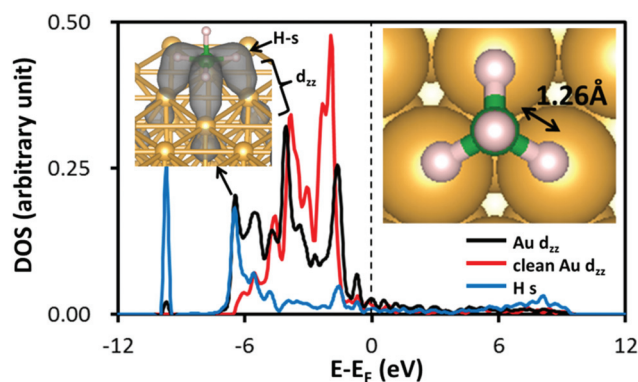


Fig. 2 The change in the density of states of the surface gold atom is prominent only for the d_{zz} component which resonates with the H-s state of the adsorbate. The inset figure shows that the mixing between charge density of the H atoms and the metal is very evident. Thus, the molecular adsorption of borohydride on Au can be described by the strong s - d_{zz} hybridization of the adsorbate–metal states.

To understand the mechanism of adsorption of borohydride on Au, we analyzed the density of states (DOS) projected on surface Au atoms and borohydride for clean and adsorbed systems. We found that the shifting and broadening of states are prominent only for the d_{zz} state of Au which hybridizes with the H-s state of borohydride. Thus, the molecular structure of borohydride on Au can be described by the s - d_{zz} hybridization of adsorbate-metal states. This is illustrated by the partial charge density distribution projected using a 0.01 electron/ a_0^3 isosurface value at an identified bonding state shown in the inset of Fig. 2. Here, the mixing between charge density of the H atoms and the metal is very evident. This hybridization is promoted when borohydride is in the H-up orientation, which explains its preferential stability over the H-down orientation.

3.2 Adsorption energetics on Au alloys

Au is known to form stable alloys such as Au_3M ($M = Cr, Mn, Fe, Co, Ni$) with the $L1_2$ structure. These alloys have been successfully synthesized in the laboratory and examined using a variety of experimental techniques, such as XRD and TEM.^{55–59} The (111) facet of these metals was used to rule out the structural differences between different surfaces and to extract meaningful trends in the properties as a function of the substrate identity. The calculated lattice constants are reported in Table 1, which are in excellent agreement with experiments.⁵⁵

Fig. 3 shows the adsorption configuration of borohydride on these surfaces in a 2×2 supercell (4 M and 12 Au atoms per layer). Borohydride tends to “seek” the alloying metal by adsorbing on the surface with B on top of the alloying metal

Table 1 Lattice constants, bond lengths and BH_4 adsorption energies on Au(111) and $Au_3M(111)$

(111) Surface	Lattice constant (Å)	B–M bond length (Å)	B–H bond length (Å)	Adsorption energy (eV)
Au_3Cr	4.07	2.07	1.28	–2.31
Au_3Mn	4.05	2.11	1.26	–2.19
Au_3Fe	4.03	2.01	1.28	–2.34
Au_3Co	4.03	1.84	1.36	–2.41
Au_3Ni	4.03	1.93	1.32	–2.16
Au	4.18	—	1.26	–1.83

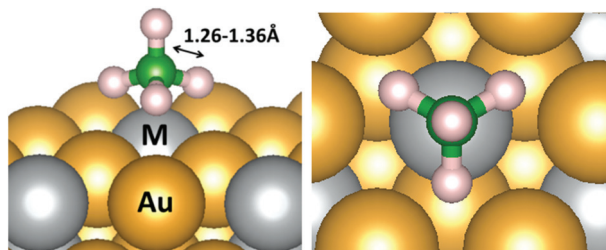


Fig. 3 Adsorption configuration of borohydride on $Au_3M(111)$ ($M = Cr, Mn, Fe, Co, Ni$) surfaces.

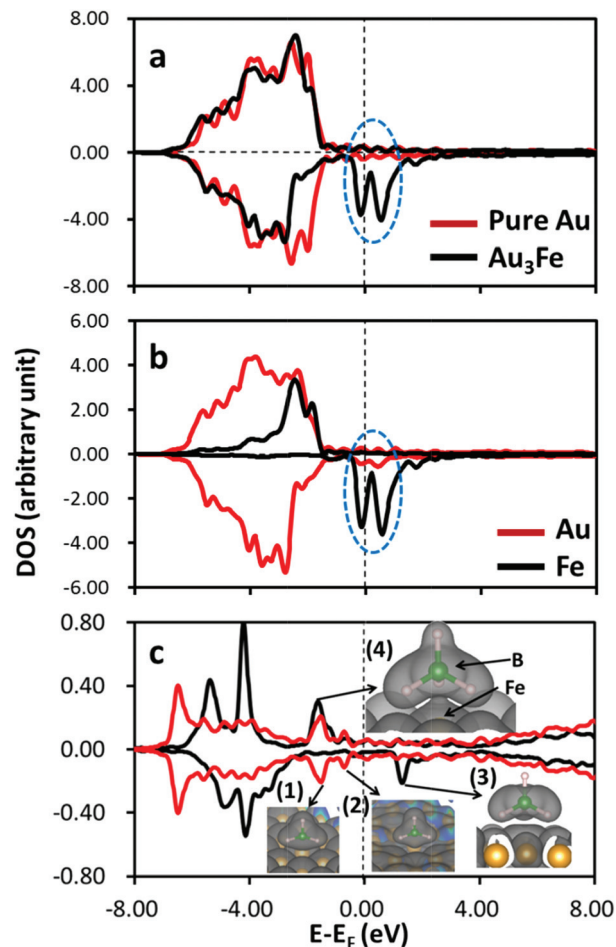


Fig. 4 (a) Surface d band projected on pure Au (red) and clean Au_3Fe (black), (b) atom projected surface d band of Au_3Fe , and (c) sp states of borohydride adsorbed on pure Au (red) and Au_3Fe (black). States near the Fermi level are shown by blue dashed ellipses in (a) and (b).

M , and H atoms on the hollow sites. B bonds directly with the alloying metal M unlike in the case of pure Au wherein the H atoms bond directly with Au atoms. These alloying metals are known to be easily oxidized⁶⁰ by transferring electron charge to an electronegative atom. This oxidation can be facilitated by the direct bonding of B with M .

For all these alloys, the adsorption energy has increased by 0.33–0.58 eV compared to the case of pure Au. To explain this, we compared the DOS projected on the surface metal atoms for pure Au and clean Au_3Fe slabs as a representative alloy (red and black curves respectively in Fig. 4a). For the case of pure Au, the d band is fully occupied. When this Au-d band hybridizes with the sp state of borohydride, the derived sp-d bonding and antibonding states are both occupied as shown in Fig. 4c (red curve). We have confirmed that the occupied states near the Fermi level (insets 1 and 2 in Fig. 4c) have antibonding characteristics which contribute to a repulsive interaction. On the other hand, for the clean Au_3Fe surface (black curve in Fig. 4a), spin-down states around the Fermi level have appeared as indicated by the dashed ellipse. We note that these states are mainly Fe states as shown in Fig. 4b. The lower

band in Fig. 4a for Au₃Fe is mainly from Au. The derived anti-bonding state of the sp–d interaction (inset 3 in Fig. 4c) is upshifted and becomes unoccupied unlike on pure Au. The corresponding bonding state below the Fermi level (inset 4 in Fig. 4c) is occupied and is due to the B–Fe bonding interaction.

We note that for the d band projected on the surface alloying metal M of other clean Au₃M slabs, there is also an emergence of states near the Fermi level in the same energy range as that for Au₃Fe. The same bonding mechanism as for the case of Au₃Fe explains the increase in the adsorption energy of borohydride on other Au₃M surfaces compared to pure Au.

3.3 Adsorption structures on Au alloys

The B–H bond lengths of borohydride on all these alloys fall within the previously set B–H bond lengths for molecular adsorption of borohydride.^{33,39} For Au₃Cr, Au₃Mn and Au₃Fe, the B–H bond lengths are almost the same as that for pure Au, while for Au₃Co and Au₃Ni, the B–H bond lengths are more elongated (Table 1). To understand this, we analyzed the DOS projected on the surface alloying atom M for the clean and adsorbed systems. In Fig. 5, we present the DOS of the Fe atom (left panel) on the surface of Au₃Fe (representing Au₃Cr, Au₃Mn and Au₃Fe alloys) and the surface Co atom (right panel) of Au₃Co (representing Au₃Co and Au₃Ni alloys). For all these alloys, the components of the d band that protrude out of the surface (d_{zz} , d_{xz} , d_{yz}) interact with borohydride. However, the shift and formation of peaks for “surface-parallel” components of the d band (d_{xy} and $d_{x^2-y^2}$) are noted only for Au₃Co and Au₃Ni. This happens because borohydride adsorbs at a closer distance to the surfaces of Au₃Co and Au₃Ni (B–M bond length in Table 1) compared to the other alloys studied. Thus,

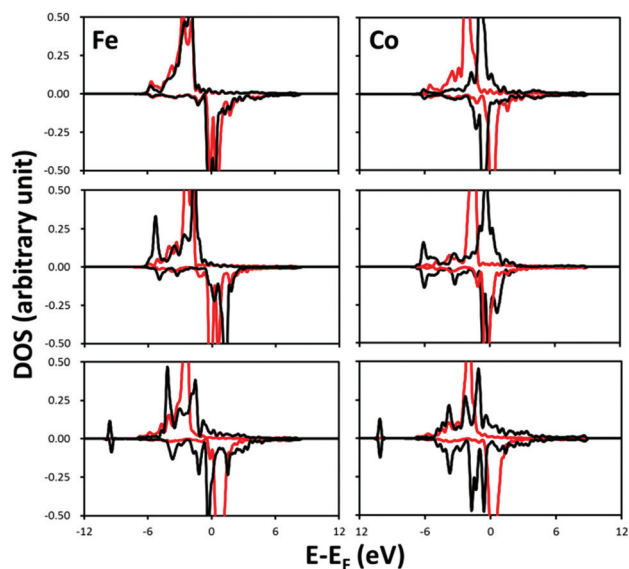


Fig. 5 Density of states projected on $d_{xy}, d_{x^2-y^2}$ (top panel), d_{xz}, d_{yz} (middle panel) and d_{zz} (bottom panel) of Fe (left panel) on the surface of Au₃Fe to represent the alloying metal on Au₃Cr, Au₃Mn and Au₃Fe groups, and the surface Co atom (right panel) of Au₃Co to represent Au₃Co and Au₃Ni. The red and black curves correspond to the clean surface and the surface with adsorbed borohydride, respectively.

the interaction of borohydride with surface-parallel components of the d band leads to further elongation of the B–H bonds on Au₃Co and Au₃Ni alloys. The magnetic moment of Co has almost diminished upon borohydride adsorption (from 1.905 μ_B to 0.293 μ_B). However, this large decrease in the magnetic moment of Co is not observed for Ni (from 0.328 μ_B to 0.111 μ_B). Thus, the demagnetization of the substrate can be ruled out as the cause of the shifting of DOS peaks (Fig. 5) for d_{xy} and $d_{x^2-y^2}$ components of the d band of Co and Ni. Further discussions in the magnetic aspects of borohydride adsorption can be found in Ref. 39.

These DFT studies shed light on the vast selections of pure and alloy catalysts for BH₄[−] oxidation. We have shown that molecular adsorption structure with greater adsorption energy compared to pure Au can be achieved on these Au-based alloys. Further studies that involve the calculation of free energies, influence of the solvent, and treatment of an externally applied electrode potential shall be done in the next steps of the research to address the electro-catalytic reactions on these surfaces.

4. Conclusion

The structure and stability of borohydride on Au(111) and Au₃M(111) (M = Cr, Mn, Fe, Co and Ni) surfaces were studied using first-principles calculations based on spin-polarized density functional theory. Borohydride adsorbs on Au(111) molecularly at lower adsorption energy compared to other transition metals previously reported. This explains why high overpotential is necessary to achieve an appreciable rate of borohydride oxidation on Au. This molecular adsorption is characterized by the strong hybridization of the H-s state of borohydride with the d_{zz} state of Au. This interaction is promoted when borohydride is adsorbed on the surface with B at the hollow site and H atoms at the top sites. Alloying Au with 3d transition metals results in greater stability of borohydride adsorption compared to pure Au. For these alloys, there is an emergence of unoccupied states in the surface d band around the Fermi level with respect to the fully occupied and low-lying d band of pure Au. Thus, the derived antibonding state of the sp–d interaction is upshifted and becomes unoccupied compared to pure Au. The difference in the B–H bond elongation of borohydride on these alloy surfaces points to the effect of the surface parallel (d_{xy} and $d_{x^2-y^2}$ states) components of the d-band of the alloying metal. On the alloy surfaces, B binds directly with the alloying metal unlike the case of pure Au wherein the surface bonding is through the H atoms. This happens in order to facilitate the oxidation of the alloying metal by transferring an electron to B. These results pose relevant insights into the design of Au-based anode catalysts for the direct borohydride fuel cell.

Acknowledgements

This work was supported in part by MEXT (Ministry of Education, Culture, Sports, Science and Technology) through the

G-COE (Special Coordination Funds for the Global Center of Excellence) program “Atomically Controlled Fabrication Technology”, Grant-in-Aid for Scientific Research on Innovative Areas Program (2203-22104008) and Scientific Research (c) (22510107) program, and JST (Japan Science and Technology Agency) through the ALCA (Advanced Low Carbon Technology Research and Development) Program. Some of the calculations were done using the computer facilities of Cyber Media Center (Osaka University), ISSP Super Computer Center (University of Tokyo), and Large Scale Simulation Program KEK No. T10-12 of the High Energy Accelerator Research Organization. R.L. Arevalo acknowledges the Ministry of Education, Culture, Sports, Science and Technology (MEXT) for a scholarship grant. M.C. Escaño acknowledges the Japan Society for Promotion of Science (JSPS) Fellowship for research funds. The authors acknowledge Prof. Elod Gyenge of The University of British Columbia (Vancouver, Canada) for fruitful collaborations.

Notes and references

- M. Contestabile, G. J. Offer, R. Slade, F. Jaeger and M. Thoennes, *Energy Environ. Sci.*, 2011, **4**, 3754.
- G. Frenette and D. Forthoffer, *Int. J. Hydrogen Energy*, 2009, **34**, 3578.
- P. Corbo, F. Migliardini and O. Veneri, *Renew. Energy*, 2009, **34**, 1955.
- H.-J. Neef, *Energy*, 2009, **34**, 327.
- D. Mori and K. Hirose, *Int. J. Hydrogen Energy*, 2009, **34**, 4569.
- J.-H. Wee, *J. Power Sources*, 2006, **161**, 1.
- Z. P. Li, B. H. Liu, K. Arai and S. Suda, *J. Alloys Compd.*, 2005, **404**, 648.
- C. P. de Leon, F. C. Walsh, D. Pletcher, D. J. Browning and J. B. Lakeman, *J. Power Sources*, 2006, **155**, 172.
- J.-H. Wee, *J. Power Sources*, 2006, **155**, 329.
- E. Gyenge, *Electrochim. Acta*, 2004, **49**, 965.
- J. I. Martins, M. C. Nunes, R. Koch, L. Martins and M. Bazzouai, *Electrochim. Acta*, 2007, **52**, 6443.
- B. H. Liu, Z. P. Li and S. Suda, *Electrochim. Acta*, 2004, **49**, 3097.
- B. H. Liu, Z. P. Li and S. Suda, *Electrochim. Acta*, 2003, **150**, A398.
- J. P. Elder, *Electrochim. Acta*, 1962, **7**, 417.
- J. P. Elder and A. Hickling, *Trans. Faraday Soc.*, 1962, **58**, 1852.
- M. E. Indig and R. N. Snyder, *J. Electrochem. Soc.*, 1962, **109**, 1104.
- H. Brown and C. A. Brown, *J. Am. Chem. Soc.*, 1962, **84**, 1493.
- M. V. Mirkin, H. Yang and A. J. Bard, *J. Electrochem. Soc.*, 1992, **139**, 2212.
- M. Chatenet, F. Micoud, I. Roche and E. Chainet, *Electrochim. Acta*, 2006, **51**, 5459.
- E. Gyenge, M. Atwan and D. Northwood, *J. Electrochem. Soc.*, 2006, **153**, A150.
- V. Lam and E. Gyenge, *J. Electrochem. Soc.*, 2008, **155**, B1155.
- V. Lam, D. Kannangara, A. Alfantazi and E. Gyenge, *J. Phys. Chem. C*, 2011, **115**, 2727.
- D. Finkelstein, N. Da Mota, J. Cohen and H. Abruna, *J. Phys. Chem. C*, 2009, **113**, 19700.
- H. Cheng and K. Scott, *Electrochim. Acta*, 2006, **51**, 3429.
- B. Molina Concha and M. Chatenet, *Electrochim. Acta*, 2009, **54**, 6119.
- B. Molina Concha, M. Chatenet, E. Ticianelli and F. Lima, *J. Phys. Chem. C*, 2011, **115**, 12439.
- M. Simoes, S. Baranton and C. Coutanceau, *Electrochim. Acta*, 2010, **56**, 580.
- M. Simoes, S. Baranton and C. Coutanceau, *J. Phys. Chem. C*, 2009, **113**, 13369.
- V. Kiran, T. Ravikumar, N. Kalyanasundaram, S. Khrishnamurthy, A. Shukla and S. Sampath, *J. Electrochem. Soc.*, 2010, **157**, B1201.
- P. He, Y. Wang, X. Wang, F. Pei, H. Wang, L. Liu and L. Yi, *J. Power Sources*, 2011, **196**, 1042.
- P. He, X. Wang, Y. Liu, L. Yi and X. Liu, *Int. J. Hydrogen Energy*, 2012, **37**, 1254.
- P. He, X. Wang, Y. Liu and L. Yi, *Int. J. Hydrogen Energy*, 2012, **37**, 11984.
- M. C. S. Escano, E. Gyenge, R. L. Arevalo and H. Kasai, *J. Phys. Chem. C*, 2011, **115**, 19883.
- G. Rostamikia and M. J. Janik, *Electrochim. Acta*, 2010, **55**, 1175.
- G. Rostamikia and M. J. Janik, *J. Electrochem. Soc.*, 2009, **156**, 1.
- J. S. Zhang and W. N. Jiang, *J. Power Sources*, 2007, **164**, 772.
- A. Y. Tsivadaze, M. R. Tarasevich, V. N. Titova, A. A. Yavich and N. V. Petrova, *Phys. Chem.*, 2007, **414**, 107.
- R. L. Arevalo, M. C. S. Escano and H. Kasai, *e-J. Surf. Sci. Nanotechnol.*, 2011, **9**, 257.
- R. L. Arevalo, M. C. S. Escano, E. Gyenge and H. Kasai, *Surf. Sci.*, 2012, **606**, 1954.
- Y. Kunisada, H. Kishi, F. Dimas, M. David, H. Nakanishi, H. Kasai, T. Asari and S. Hayashi, *Jpn. J. Appl. Phys.*, 2010, **49**, 02BB04.
- H. Xin and S. Linic, *J. Chem. Phys.*, 2010, **132**, 221101.
- J. Roques and A. Anderson, *J. Electrochem. Soc.*, 2004, **151**, E85.
- G. Kresse and J. Furthmuller, *Comput. Mater. Sci.*, 1996, **6**, 15.
- G. Kresse and J. Furthmuller, *Phys. Rev. B: Condens. Matter*, 1996, **54**, 11169.
- G. Kresse and J. Hafner, *Phys. Rev. B: Condens. Matter*, 1993, **47**, 558.
- G. Kresse and J. Hafner, *Phys. Rev. B: Condens. Matter*, 1994, **49**, 14251.
- P. E. Blochl, *Phys. Rev. B: Condens. Matter*, 1994, **50**, 17953.
- G. Kresse and J. Joubert, *Phys. Rev. B: Condens. Matter*, 1999, **59**, 1758.

- 49 J. Perdew, K. Burke and M. Ernzerhof, *Phys. Rev. Lett.*, 1996, **77**, 3865.
- 50 J. Perdew, K. Burke and M. Ernzerhof, *Phys. Rev. Lett.*, 1997, **78**, 1396.
- 51 H. J. Monkhorst and J. D. Pack, *Phys. Rev. B: Solid State*, 1976, **13**, 5188.
- 52 M. Methfessel and A. Paxton, *Phys. Rev. B: Condens. Matter*, 1989, **470**, 3616.
- 53 I. Stich, R. Car, M. Parrinello and S. Baroni, *Phys. Rev. B: Condens. Matter*, 1989, **39**, 4997.
- 54 B. Hammer and J. K. Norskov, *Nature*, 1995, **376**, 238.
- 55 Y. Vasquez, Z. Luo and R. E. Schaak, *J. Am. Chem. Soc.*, 2008, **130**, 11866.
- 56 K. Yamamoto, *Phys. Status Solidi*, 1980, **59**, 767.
- 57 J. Dutkiewicz and G. Thomas, *Metall. Trans. A*, 1975, **6**, 1920.
- 58 H. Sato and R. S. Toth, *J. Phys. Chem. Solids*, 1966, **27**, 413.
- 59 H. Sato, R. S. Toth and G. Honjo, *J. Phys. Chem. Solids*, 1967, **28**, 139.
- 60 *CRC Handbook of Chemistry and Physics*, CRC Press, Boca Raton, FL, 92nd edn, 2011–2012, Ionization Energies of Atoms and Atomic Ions, pp. 10–196.